Switching Behavior of Class-E Power Amplifier and Its Operation Above Maximum Frequency

Seunghoon Jee, Junghwan Moon, *Student Member, IEEE*, Jungjoon Kim, Junghwan Son, and Bumman Kim, *Fellow, IEEE*

***Abstract*—The switching behavior of Class-E power amplifiers (PAs) is described. Although the zero voltage switching can be performed properly, the $C_{\rm out}$ charging process at the switch-off transition cannot be abrupt and the waveform deviates from the ideal shape, degrading the efficiency. For the operation above maximum frequency, the charging process should be even faster but it cannot follow. Moreover, the discharging process is not sufficiently fast and further degrades the efficiency. The discharging process is assisted by the bifurcated current at saturation. The performance of the Class-E PA above the maximum frequency is enhanced by the nonlinear $C_{\rm out}$, which helps to shape the voltage waveform. The bifurcated current itself cannot generate enough of a second-harmonic voltage component to shape the required voltage waveform. The performance of the Class-E PA can be further improved by a second-harmonic tuning and a conjugate matched output load, leading to the saturated PA. Compared with the Class-E PA, the saturated amplifier delivers higher output power and efficiency. A highly efficient saturated amplifier is designed using a Cree GaN HEMT CGH40010 device at 3.5 GHz. It provides a drain efficiency of 75.8% at a saturated power of 40.2 dBm (10.5 W).**

***Index Terms*—Drain efficiency, gallium nitride, load-pull simulation, power-added efficiency (PAE), power amplifier (PA).**

I. Introduction

FOR modern wireless communication systems, a power amplifier (PA) with high efficiency is essential to reduce dc power consumption and the size of the heat sink. To achieve a high-efficiency PA, several circuit topologies have been introduced. Among the topologies, Class-F, Class-E, and Class-J are the most promising ones [1]–[8]. For the Class-F PA, high efficiency is achieved by generating a rectangular voltage waveform and a half-sine current waveform through harmonic load manipulation. However, it is difficult to make the open-circuit condition that is required for the odd-harmonic loads because the large $C_{\rm out}$ creates a short circuit and the nonlinear $C_{\rm out}$ cannot be tuned out properly during the output swing, generating a looping on the load-line [2]–[4]. For the class-J PA proposed by Cripps *et al.* [1], [5], the fundamental voltage component can be increased by a factor of $\sqrt{2}$ by the second-harmonic tuning [8]–[11]. However, the efficiency of the Class-J PA is the same as that of the Class-B PA due to the phase mismatch between the fundamental components of the current and voltage waveforms reducing the output power and efficiency. A comparison between the Class-J PA and the optimized amplifier, a saturated amplifier, is explained in [8].

The Class-E PA can deliver the highest efficiency among the topologies because this amplifier tunes all harmonic impedances through the L–C series resonator, making the ideal crossover from the conduction state to the off-state of the transistor without having discharging loss. Although the power density is lower, the amplifier can be realized through the ideal switching operation with a simple matching network [6], [7]. However, the ideal switching operation is not possible even at a low frequency, because it requires an abrupt charge build-up on $C_{\rm out}$ at the switching off transition. At a high frequency, above the maximum operation frequency ($f_{\max,E}$) of the ideal Class-E, the discharging process of $C_{\rm out}$ is not sufficiently fast, and residual charge at the switch-on transition is discharged through the bifurcated current at the saturated operation, thus degrading the overall efficiency significantly [13]. To achieve the high efficiency of the Class-E PA beyond $f_{\max,E}$, optimization of the voltage waveform with assumption of the conventional Class-E current waveform and linear $C_{\rm out}$ was proposed [14], [15]. However, we have found that the current waveform cannot be maintained above the $f_{\max,E}$ but is significantly deviated from that of the ideal case. Moreover, $C_{\rm out}$ is highly nonlinear and there have been some efforts to analyze Class-E operation with nonlinear $C_{\rm out}$, but they only focus on operation at a low frequency below $f_{\max,E}$ [16]–[18].

In this paper, the Class-E PA with the nonlinear $C_{\rm out}$ is analyzed for operation above $f_{\max,E}$. For the operation at a frequency more than two times of $f_{\max,E}$, the ideal switching operation of the Class-E is not possible, and switching is assisted by the bifurcated current generated by the gm-driven saturated mode. This operation mode can provide high efficiency, but it is not an optimal structure. The saturated amplifier, described in [8], [19], and [20], is the optimized version of the Class-E PA in the high-frequency region. This amplifier may be identical to the harmonic tuned PA reported in [11] and [12]. However, they just figure out the second- and third-harmonic loads for the maximum efficiency without investigating the fundamental behavior. We have compared the Class-E PA and the saturated amplifier in terms of efficiency and output power. The entire analysis is carried out using a simplified transistor model. To

Manuscript received July 21, 2011; revised September 22, 2011; accepted September 23, 2011. Date of publication December 01, 2011; date of current version December 30, 2011. This work was supported in part by The Ministry of Knowledge Economy, Korea, under the Information Technology Research Center support program supervised by the National IT Industry Promotion Agency under Grant NIPA-2011-(C1090-1111-0011), the World Class University program through the National Research Foundation of Korea funded by the Ministry of Education, Science and Technology under Grant R31-2010-000-10100-0, and the Brain Korea 21 Project in 2011.

The authors are with the Department of Electrical Engineering and Information Technology Convergence Engineering, Pohang University of Science and Technology, Pohang 790-784, Korea (e-mail: cshcomit@postech.ac.kr; jhmoon@postech.ac.kr; jungjoon@postech.ac.kr; jhson@postech.ac.kr; bmkim@postech.ac.kr).

Digital Object Identifier 10.1109/TMTT.2011.2173208

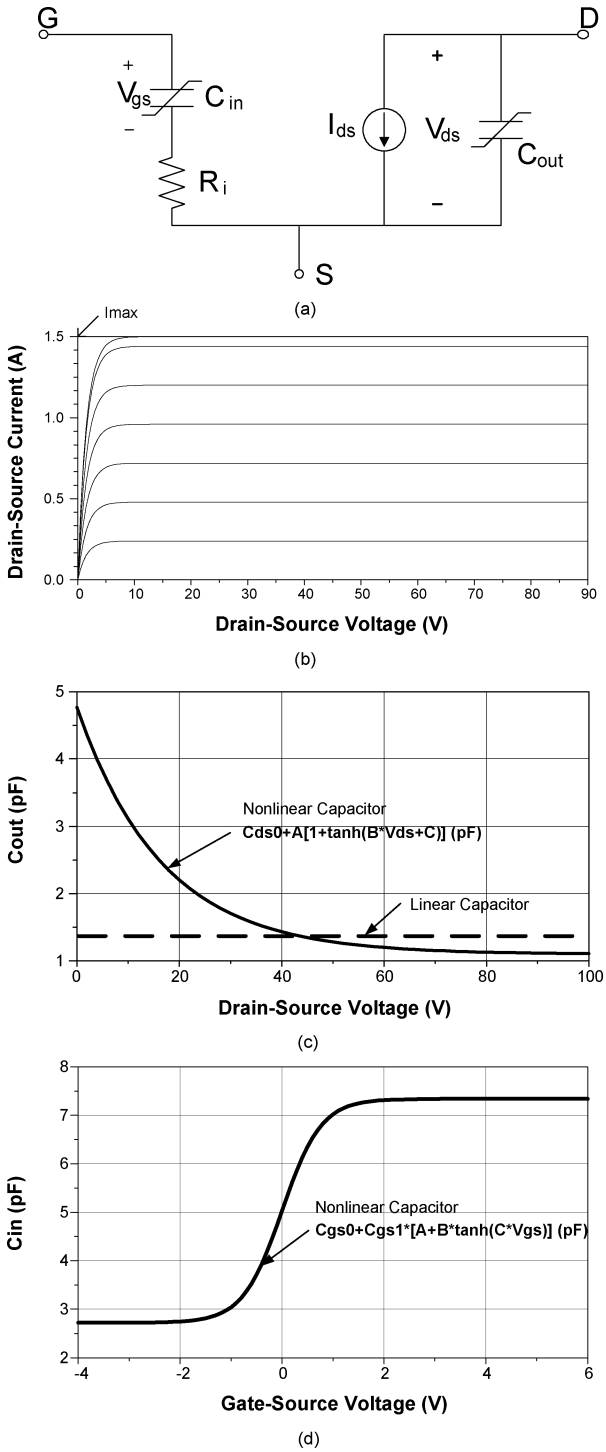

Fig. 1. (a) Ideal transistor model using the symbolically defined device. (b) DC–I–V characteristic. (c) Capacitances for the linear and nonlinear $C_{\rm out}$s. (d) Capacitances for nonlinear $C_{\rm in}$.

validate the ideal simulation, the behaviors of the Class-E PA and saturated amplifiers above $f_{\max,E}$ are simulated using a real device model of Cree GaN HEMT CGH60015. From the simulation results described in Section IV-B, we demonstrate that the extracted waveforms are very similar to that of the simplified transistor case, verifying the ideal simulation. The simulation results clearly show that the saturated amplifier provides

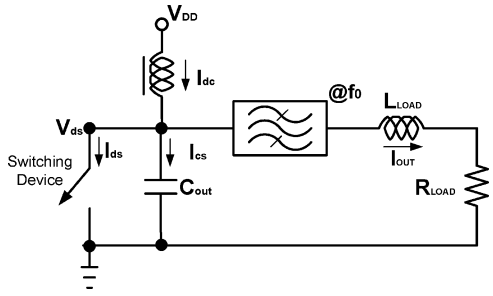

Fig. 2. Conventional circuit of a Class-E PA.

excellent output power and efficiency compared with those of the Class-E PA.

II. Analysis of the Class-E PA

A. Ideal Transistor Model

To explore the fundamental behavior of the Class-E PA, we construct an ideal transistor model in the Agilent's Advanced Design System (ADS) using a symbolically defined device [8]. The ideal transistor parameters for $I_{\max}$, V_k, linear $C_{\rm out}$, and R_i are set to 1.5 A, 4 V, 1.4 pF, and 3 Ω, respectively, as shown in Fig. 1. The nonlinear $C_{\rm out}$ consists of a gate–drain capacitor $C_{\rm gd}$ with the Miller effect and a drain–source capacitor $C_{\rm ds}$. The nonlinear $C_{\rm in}$ includes $C_{\rm gs}$ and $C_{\rm gd}$ with the input Miller effect. These parameters are extracted from the model of the Cree GaN HEMT CGH60015 device. $C_{\rm gd}$ has a very nonlinear characteristic depending on the drain–source voltage $V_{\rm ds}$, and $C_{\rm gs}$ depends on the gate–source voltage $V_{\rm gs}$ [16].

The maximum frequency of the Class-E operation is limited by $I_{\max}$, $C_{\rm out}$, and $V_{\rm dc}$ and is expressed by the following [13]:

$$f_{\max,E} = \frac{I_{\rm dc}}{2\pi^2 \cdot C_{\rm out} \cdot V_{\rm dc}} \approx \frac{I_{\max}}{56.5 \cdot C_{\rm out} \cdot V_{\rm dc}.} \qquad (1)$$

For large power generation, a large device should be employed to increase $I_{\max}$, but $C_{\rm out}$ also increases proportional to $I_{\max}$, and $I_{\max}/C_{\rm out}$ is a fixed value for a given process. In addition, $V_{\rm dc}$ should be the maximum rated value of the device to generate the maximum output power. Therefore, $f_{\max,E}$ is a process-dependent constant value. Based on the above parameters, the maximum frequency of this device is 730 MHz when $V_{\rm dc}$ is 26 V. In this model, the breakdown voltage is set to 100 V, which can sustain the maximum voltage swing of the Class-E PA, which is 3.56 $\cdot V_{\rm dc} \approx 92.6$ V.

B. Basic Operation of a Conventional Class-E PA

The Class-E PA consists of a switching device, a bandpass filter, and a series load $(R_{\rm LOAD} + {\rm j}X_{\rm LOAD})$, as shown in Fig. 2. There is no power dissipation in the device because the current does not flow through the device when the switch is in the off-state, and the voltage cannot build across the switching device when the switch is in the on-state. Therefore, the Class-E PA has 100% efficiency under ideal conditions: zero on-resistance, ideal switching operation, and high-Q bandpass filter. The current and voltage waveforms of the Class-E PA with a linear

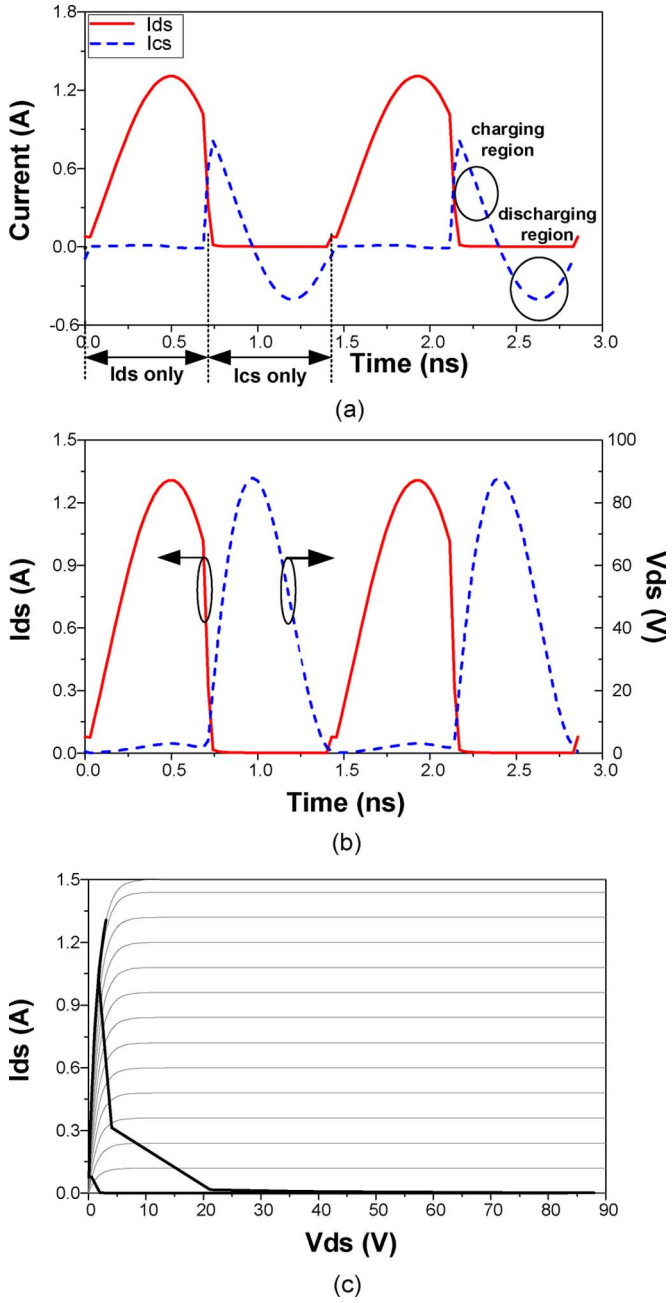

Fig. 3. Operation behavior of the conventional Class-E PA driven by rectangle pulse input. (a) Current profiles. (b) Current and voltage waveforms. (c) Load-line.

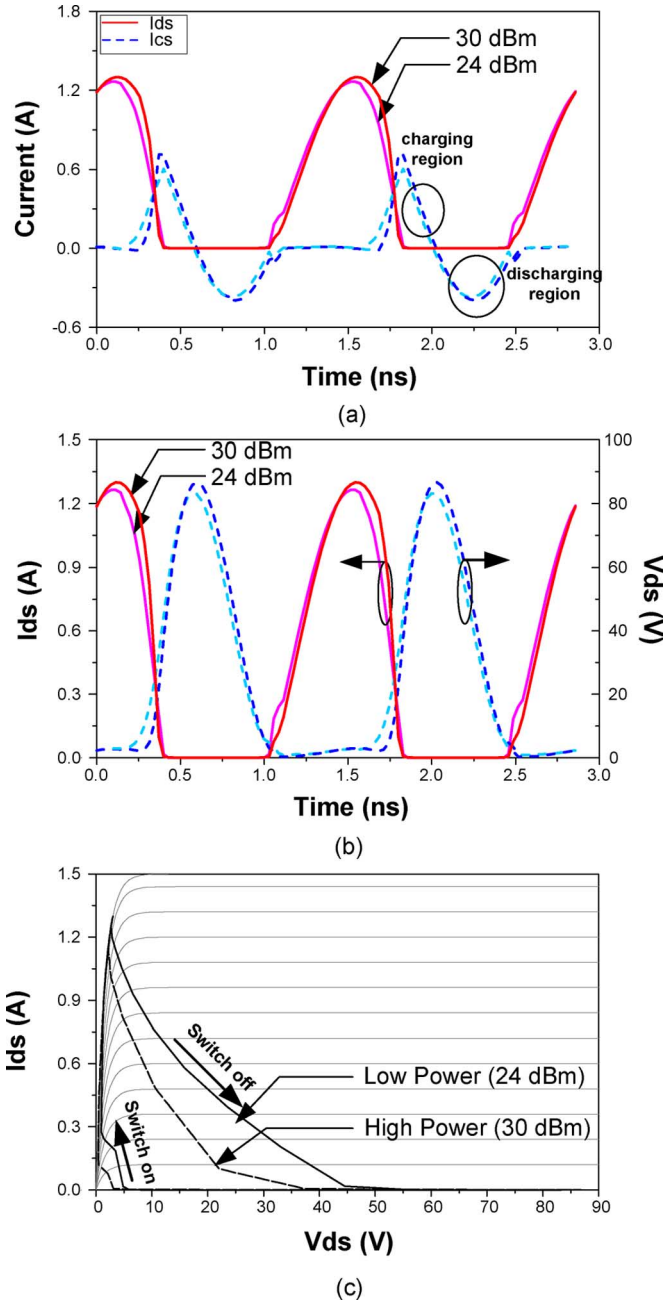

Fig. 4. Operation behavior of the conventional Class-E PA with two sinusoidal input drives levels: 24 and 30 dBm. (a) Current profiles. (b) Current and voltage waveforms. (c) Load lines.

output capacitance and a rectangular pulse drive are simulated at 700 MHz using the model with $Q = 7$ in Fig. 2, whose switch follows the I–V curve in Fig. 1(a). The resulting waveforms are depicted in Fig. 3. They are very close to those of the ideal case. However, we can clearly see the nonideal switching with looping from the load-line shown in Fig. 3(c), because the capacitance$(C_{\rm out})$ cannot support the required current at the transition state from the switch-on to the switch-off, which is a depleted state of the $C_{\rm out}$. This charge build-up process should be very fast, but the switch cannot respond that fast because of the $\mathrm{R}C_{\rm out}$ constant whose R is large as determined by the load-line. However, the zero-voltage switching is carried out very accurately because the $C_{\rm out}$ is already depleted. Because of the finite on-resistance of 2 Ω and the nonideal switching, the calculated efficiency is 91.6% with an output power of 40.3 dBm.

Generally, the transistor cannot be driven by the pulse at a high frequency because the harmonics are cut off at the input by the finite R_i and the input capacitance $(C_{\rm in})$. Thus, to consider the real operation, the Class-E PA is simulated with a sinusoidal input drive, and the resulting current and voltage waveforms and load-lines are shown in Fig. 4. As we described earlier, the zero-voltage-switching (ZVS) and zero-voltage-derivative-switching (ZVDS) conditions can be satisfied since discharging the capacitor is fast enough to lower the $V_{\rm ds}$ to near zero. However, the turn-off process has a bigger problem because the slower

sinewave drive generates an even larger load resistor. Compared with the pulsed input condition, the efficiency is decreased to 85.5% or 90%, depending on the input drive level. The efficiency can be increased with a large input drive condition with a reduced gain because of the faster charging process.

III. Operation of Class-E PA Beyond Maximum Operation Frequency

A. Operation of the Class-E PA Near $f_{\max,E}$ With Linear $C_{\rm out}$

For the Class-E PA operation above $f_{\max,E}$, the conventional current waveform of the Class-E PA cannot be retained because the capacitor cannot be charged or discharged fast enough to support the required voltage waveform. To investigate the operation of the Class-E PA near $f_{\max,E}$, we simulate the Class-E PA with an input power of 24 dBm (lower power case in Fig. 4) at 0.9, 1.5, and 2.1 GHz, which are 1.2, 2.1, and 2.9 times larger than $f_{\max,E}$. The matching circuit topology is identical to the previous case, but the fundamental load is optimized for the maximum efficiency at an output power of 40 dBm. Fig. 5 shows the current and voltage waveforms of the Class-E PA at each frequency. At 0.9 GHz, the operation of the Class-E PA is similar to that of the conventional Class-E PA case, as shown in Fig. 4. The turn-off transition times remain almost a constant for the three cases, indicating that the transition is governed by the *RC* time constant. However, the ZVDS cannot be satisfied at the turn-on process for the operation above $f_{\max,E}$ because the charge in the capacitor cannot be discharged sufficiently quickly. The remaining charge at the transition state is discharged very quickly through on-resistance, thus creating the bifurcated current. The efficiency of the class-E operation of $f_{\max,E}$ is decreased because of the large internal power consumption at the on and off transitions, as shown in Fig. 6. From the simulation results, we can see that the behavior of the Class-E PA significantly deviates from that of the ideal case for frequencies above 1.5 GHz, which is about 2.1 times $f_{\max,E}$. The power performances are summarized in Table I.

B. Operation of the Class-E PA at Far Above $f_{\max,E}$ With Linear $C_{\rm out}$

To optimize the Class-E operation beyond $f_{\max,E}$, we designed the amplifier at 3.5 GHz, which is 4.7 times larger than the $f_{\max,E}$ of the conventional Class-E operation. The fundamental-harmonic load-pull simulation is carried out using Agilent ADS to achieve maximum efficiency. All harmonic output impedances are open, and a sinusoidal input is provided with $I_{\rm dsq} = 0.3$ A, which is a class-AB bias to increase power-added efficiency (PAE) at high frequency. From the simulation, the best performance is achieved when the Class-E PA has a bifurcated current waveform with a large second-harmonic component, which can help to shape the drain voltage waveform as shown in Fig. 7. This behavior is quite different from that of the conventional Class-E PA because the transistor cannot operate as an ideal switch at the high frequency because of the *RC* time-related switching operation. To build up the voltage waveform across $C_{\rm out}$, the transistor is pushed into the saturated region. The quasi-ZVS and ZVDS occurs at the bifurcated current point A in Fig. 7. From there, the voltage increases slowly as it follows the on-resistance. From point B, the transistor gradually gets into the off-state, raising the voltage due to the slow charging process of the capacitor at the turn-off transition. The capacitor cannot be discharged enough at the off-state, and the bifurcated current (see the C point) assists to complete the discharging process. In this step, the bifurcated drain current enhances the negatively flowing current through the capacitor. The increased negative current enhances the turn-off sharpness. As mentioned earlier, due to the reduced R of the switch in the saturated region, the discharging process becomes faster. From the simulation results, we can see that the high efficiency of the Class-E PA beyond $f_{\max,E}$ is sustained by the bifurcated current waveform.

For efficient operation of the Class-E PA beyond $f_{\max,E}$, the fundamental load of the Class-E PA should be increased because of the enlarged fundamental voltage and reduced fundamental current, which is caused by the bifurcated current during the saturated operation. In this simulation, the fundamental load is set to 56.2 Ω, which is 1.1 times larger than that of the conventional Class-E PA. Fig. 8 shows the simulated time-domain voltage and current waveforms and load-lines of the Class-E PA according to the input power level. The operation is similar to a gm-drive saturated amplifier. The performances of the Class-E PA are summarized in Table II.

C. Operation of a Class-E PA Beyond Maximum Operation Frequency With Nonlinear $C_{\rm out}$ and $C_{\rm in}$

To consider a real device case, we have simulated the Class-E PA using the ideal model with nonlinear $C_{\rm out}$ and $C_{\rm in}$, which are described in Section II-A. The nonlinear $C_{\rm in}$ does not produce any significant second-harmonic current because the major harmonic current source is the bifurcated operation. However, the nonlinear $C_{\rm out}$ generates a large out-of-phase second-harmonic voltage component, as shown in Table II [8]. Due to the increased second-harmonic voltage component, the fundamental voltage increases with the increased fundamental load impedance. In this simulation, the fundamental load is set to 70.4 Ω, which is determined from the fundamental load-pull simulation. The voltage and current waveforms in Fig. 9 indicate that, even though the nonlinear $C_{\rm out}$ generates the second-harmonic voltage component to shape the drain–source voltage, the bifurcated current is necessary to shape the current waveform to minimize the overlap between $V_{\rm ds}$ and $I_{\rm ds}$, enhancing the efficiency. Due to the voltage waveform shaping by the nonlinear $C_{\rm out}$, the efficiency is improved.

IV. Optimization of a Class-E PA Beyond Maximum Frequency and Verification

A. Saturated Amplifier

To further optimize the Class-E PA, fundamental and second-harmonic loads are tuned. The optimized fundamental load at the current source is purely resistive with a large value, and the second-harmonic load is inductive instead of the open circuit, which is the harmonic-matching circuit for the conventional Class-E PA. The resulting amplifier, which we call the saturated amplifier [19], [20], provides the highest efficiency due to the well-shaped voltage waveform. We believe

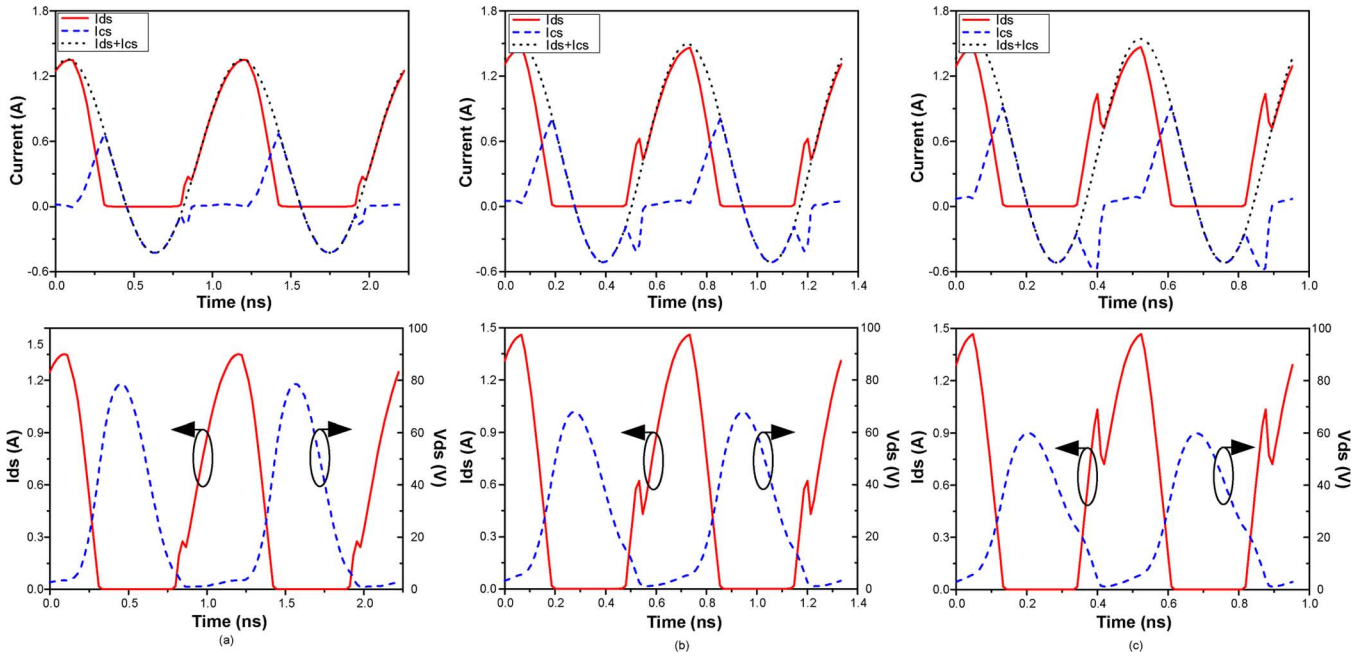

Fig. 5. Current and voltage waveforms of the Class-E PA beyond $f_{\max,E}$ with linear $C_{\rm out}$ at (a) 0.9 GHz (b) 1.5 GHz, and (c) 2.1 GHz.

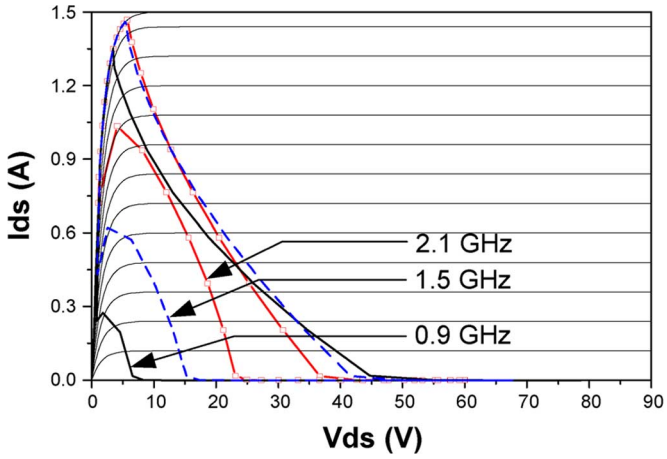

Fig. 6. Load lines of the Class-E PA beyond $f_{\max,E}$ with linear $C_{\rm out}$ at each frequency.

TABLE I
PERFORMANCE OF CLASS-E PA AT EACH FREQUENCY WITH AN INPUT POWER OF 24 dBm

	Output Power	DE
0.9 GHz	40.0 dBm	82.6%
1.5 GHz	39.9 dBm	77.0%
2.1 GHz	39.9 dBm	73.9%

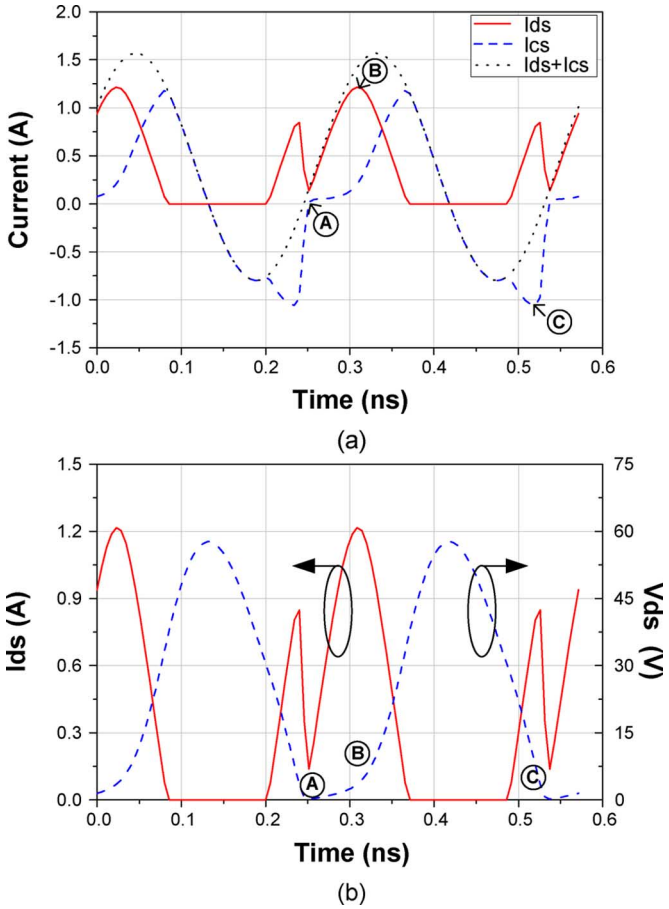

Fig. 7. (a) Current profiles and (b) current and voltage waveforms of the Class-E PA beyond $f_{\max,E}$ with linear $C_{\rm out}$.

that this amplifier is the optimized one for efficiency at the saturated operation and may be identical to the PA reported in [11] and [12] optimized by the harmonic load-pull technique. Fig. 10 shows the simulated second-harmonic load-pull contours for the output power and efficiency when the fundamental impedance is the same as that of the Class-E PA with the nonlinear $C_{\rm out}$ case in Section III-C. In the simulation, the average fundamental nonlinear $C_{\rm out}$ is 2.05 pF, and the second-harmonic load impedance that has the highest efficiency is $0.03 + j20.36\ \Omega$, which tunes out the nonlinear $C_{\rm out}$

TABLE II
COMPARISON OF A CLASS-E PA WITH LINEAR $C_{\rm out}$ AND NONLINEAR $C_{\rm out}$ AND $C_{\rm in}$

	$v_{ds,2f0}/v_{ds,1f0}$	$v_{ds,1f0}$	$i_{ds,1f0}$	$i_{ds,2f0}$	Fundamental Impedance	Output Power	DE
Class-E PA with linear C_{out}	$0.09\angle 177°$	29.45 V	0.54 A	0.18 A	$56.2\angle 19°\ \Omega$	38.6 dBm	72.9%
Class-E PA with nonlinear C_{out} and C_{in}	$0.23\angle 181°$	31.98 V	0.45 A	0.15 A	$70.4\angle 18°\ \Omega$	38.5 dBm	74.0%

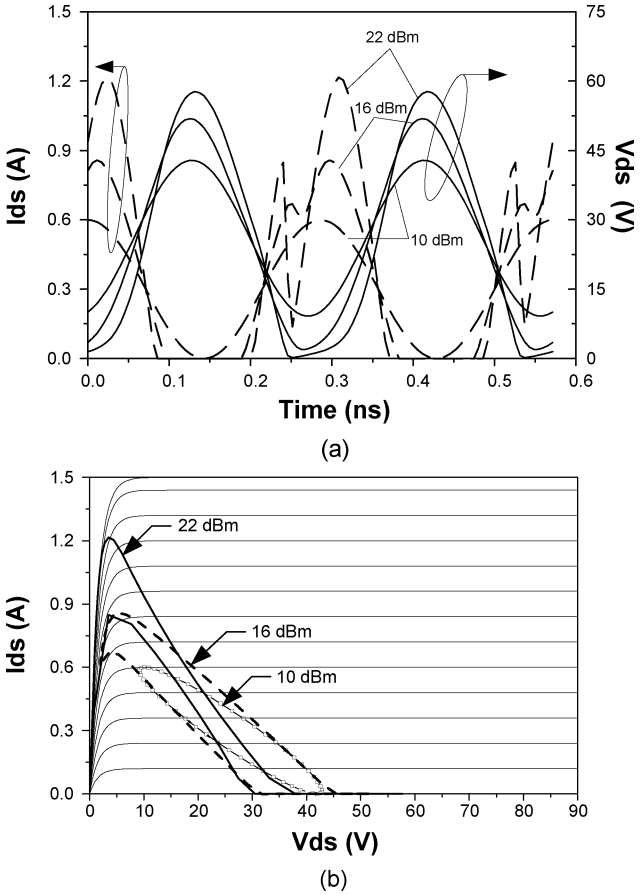

Fig. 8. Simulated (a) time-domain voltage and current waveforms and (b) load-lines of the Class-E PA with linear $C_{\rm out}$ at 3.5 GHz.

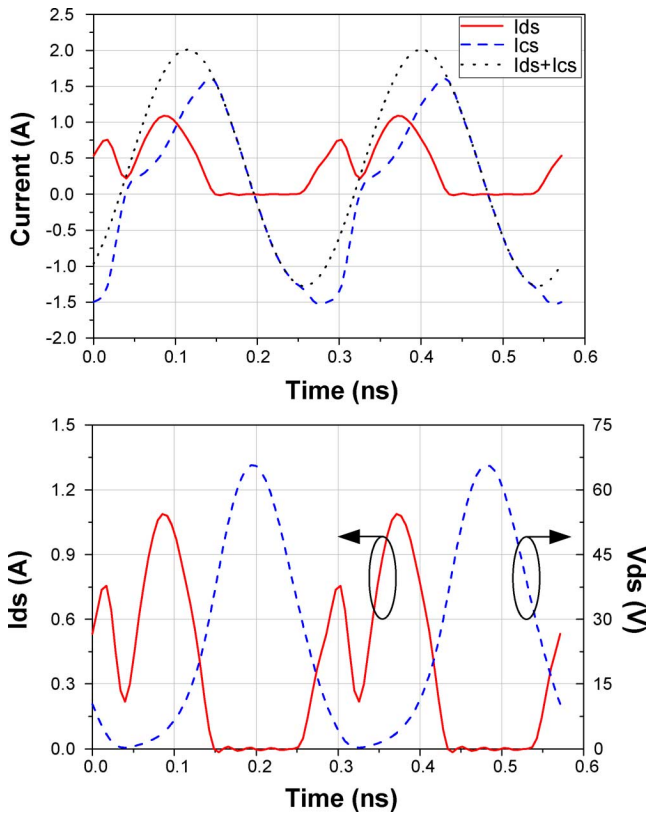

Fig. 9. Current and voltage waveforms of Class-E PA beyond $f_{\max,E}$ with nonlinear $C_{\rm out}$ and $C_{\rm in}$.

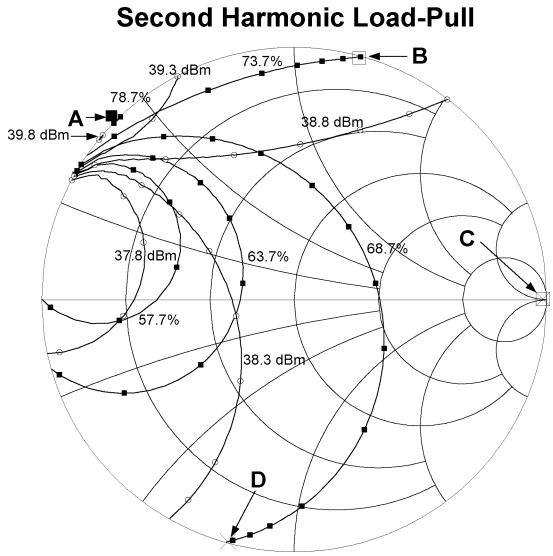

Fig. 10. Second-harmonic load-pull result of the ideal transistor with nonlinear $C_{\rm out}$ and $C_{\rm in}$.

of $-j22.72\ \Omega$. To investigate the effect of the second-harmonic load impedance, we explore the drain–source voltage waveform for the second-harmonic impedances at the marked points on the Smith chart in Fig. 10. Due to the tuned second-harmonic load, the out-of-phase second-harmonic voltage is increased, and the fundamental voltage component and efficiency are also increased [11]. Our summary results, given in Table III and Fig. 11, show clearly the behavior.

Fig. 12 shows the waveforms of the saturated amplifier with the optimum fundamental and second-harmonic loads. We cannot see the zero voltage switching observed in the Class-E operation in Fig. 9. The waveforms are similar to the inverse Class-F PA and contain higher fundamental current and voltage components, thus delivering better power performance than that of the Class-E PA. Fig. 13 shows the load-lines of the two amplifiers. The load-lines clearly show that the Class-E PA operates as a switch amplifier assisted by bifurcated current while the saturated amplifier is a gm-driven amplifier. Table IV summarizes the performances of the Class-E PA and the saturated amplifier with nonlinear $C_{\rm out}$ and $C_{\rm in}$. From the results, we can see that the fundamental load at the current is purely resistive, the out-of-phase second-harmonic voltage

TABLE III
COMPARISON OF DRAIN VOLTAGE COMPONENT AT THE MARKED POINTS ON THE SMITH CHART IN FIG. 10

Second harmonic load	$v_{ds,2f0}/v_{ds,1f0}$	$v_{ds,1f0}$	DE	Fundamental Impedance	Second Impedance	Output Power
A	$0.45\angle 179.0°$	36.26 V	80.9%	$63.7\angle 23.1°\ \Omega$	$163.6\angle -97°\ \Omega$	39.5 dBm
B	$0.27\angle 180.1°$	32.97 V	76.1%	$69.3\angle 19.4°\ \Omega$	$65.6\angle -71°\ \Omega$	38.7 dBm
C (Class-E PA)	$0.23\angle 180.4°$	31.98 V	74.0%	$70.5\angle 17.7°\ \Omega$	$50.4\angle -68°\ \Omega$	38.5 dBm
D	$0.18\angle 180.7°$	31.03 V	71.3%	$71.6\angle 15.8°\ \Omega$	$36.1\angle -64°\ \Omega$	38.2 dBm

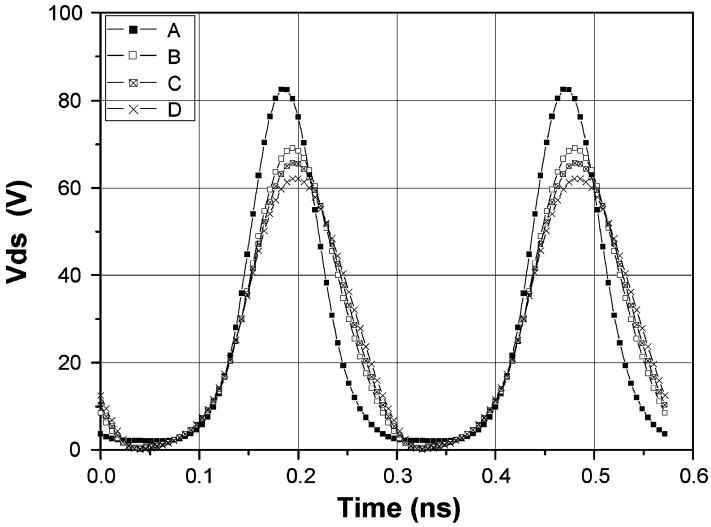

Fig. 11. Waveforms of drain voltage at the marked points on the Smith chart in Fig. 10.

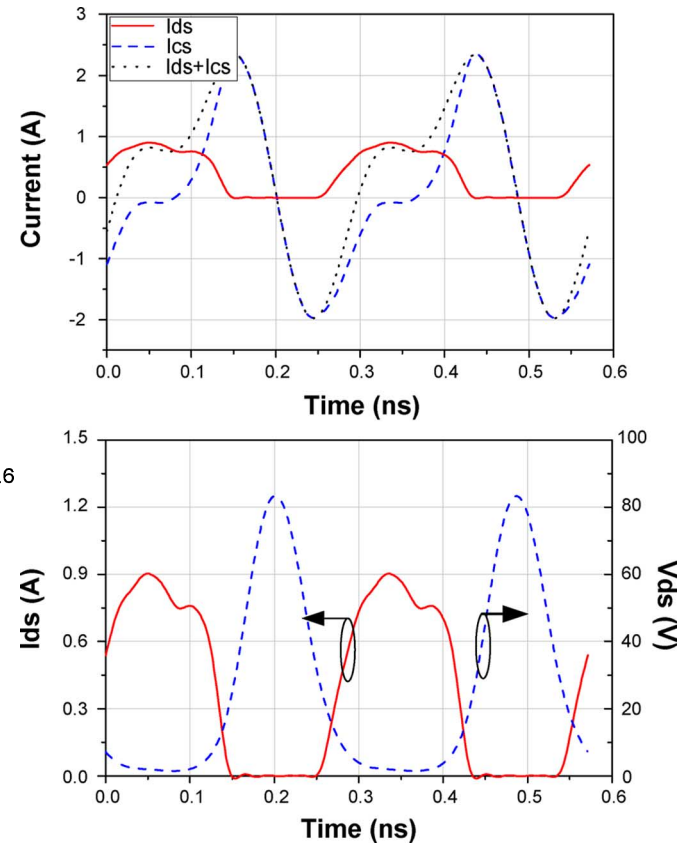

Fig. 12. Current and voltage waveforms of the saturated amplifier.

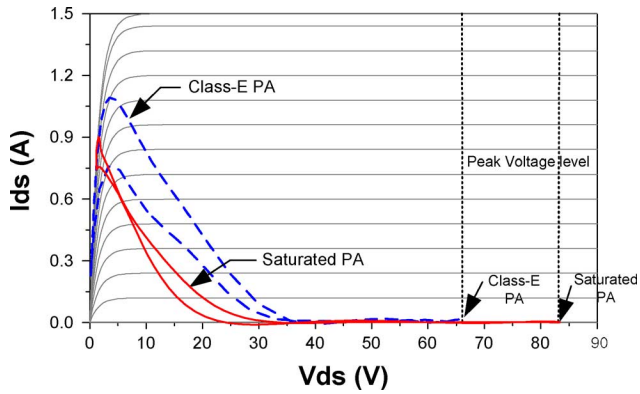

Fig. 13. Load-lines of the Class-E and saturated amplifiers with nonlinear capacitors.

component is increased by the harmonic generation of the nonlinear C_{out}, and the largest value can be achieved when the second-harmonic output load tunes out the output capacitance. Due to the large out-of-phase second voltage component, the fundamental voltage increases as the fundamental current component increases. Therefore, the saturated amplifier delivers higher output power and efficiency with proper voltage shaping. However, a better performance is obtained at the expense of the larger voltage swing.

B. Comparison of the PA Operations With the Ideal Transistor and Real Device

Thus far, we have investigated the characteristics of the Class-E and the saturated amplifiers using the simplified model. To validate the study, we design two amplifiers at 3.5 GHz using a Cree GaN HEMT CGH60015 bare chip model using an ADS simulator. I_{dsq} and V_{ds} are set to 150 mA and 26 V, respectively. The fundamental source impedance is provided by the source-pull simulation with a shorted harmonic input load [8]. As described in Section II-C, the fundamental load-pull simulation is carried out with the open harmonic load. To realize the saturated amplifier, the second-harmonic load-pull simulation is also carried out using the identical fundamental load with the Class-E case. As depicted in Fig. 14, the second-harmonic load-pull result is quite similar to the ideal case shown in Fig. 10. Fig. 15 shows the waveforms of the two amplifiers simulated using the real device, and those waveforms are very similar to those of the ideal transistor case. From the real device simulation, we can claim that the behavior of the saturated amplifier evaluated with the simplified model is accurate. The saturated amplifier generates a higher fundamental voltage component with a larger second-harmonic voltage. The current waveform, which is quite similar to that shown in Fig. 12, has a larger fundamental current because the current

TABLE IV
COMPARISON OF CLASS-E AND SATURATED PA AT THE SAME INPUT POWER WITH AN IDEAL TRANSISTOR

Circuit topology	$v_{ds,2f0}/v_{ds,1f0}$	$v_{ds,1f0}$	$i_{ds,1f0}$	Fundamental Impedance	DE	Output Power
Saturated amplifier	$0.44\angle 177.8°$	36.80 V	0.50 A	$73.2\angle 0.5°\ \Omega$	85.5%	39.4 dBm
Class-E PA	$0.23\angle 180.4°$	31.98 V	0.45 A	$70.5\angle 17.7°\ \Omega$	74.0%	38.5 dBm

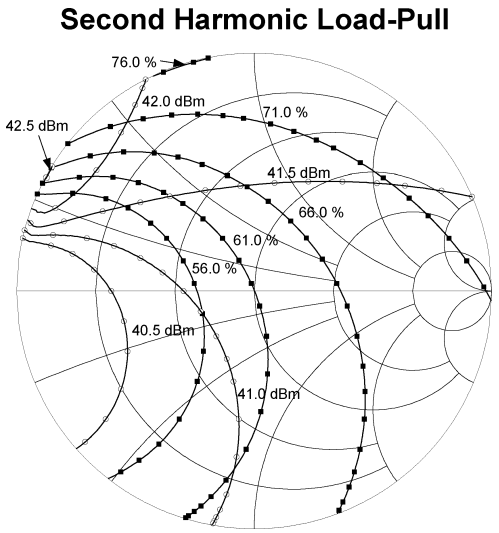

Fig. 14. Second-harmonic load-pull result of CGH60015 bare chip model.

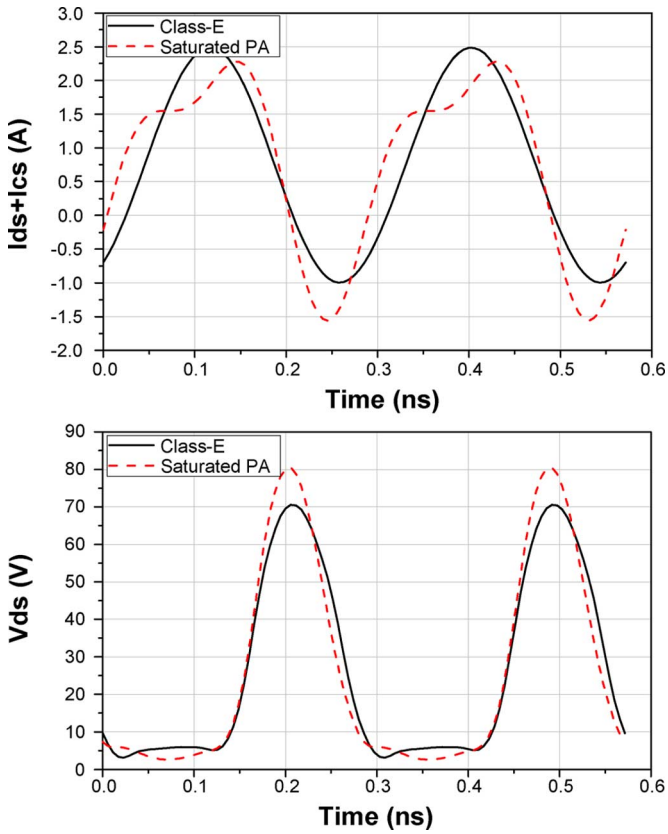

Fig. 15. Waveform of the Class-E PA and saturated amplifier for CGH60015 bare chip model.

waveform is less bifurcated. Therefore, the output power of the saturated amplifier is higher than that of the Class-E PA. The performances are summarized in Table V.

TABLE V
COMPARISON OF CLASS-E AND SATURATED PA WITH CGH60015 BARE CHIP MODEL

	$V_{ds,2f0}/V_{ds,1f0}$	$V_{ds,1f0}$	Output Power	DE
Class-E PA	$0.42\angle 181°$	32.31 V	41.4 dBm	72.1%
Saturated PA	$0.46\angle 179°$	35.03 V	41.9 dBm	79.5%

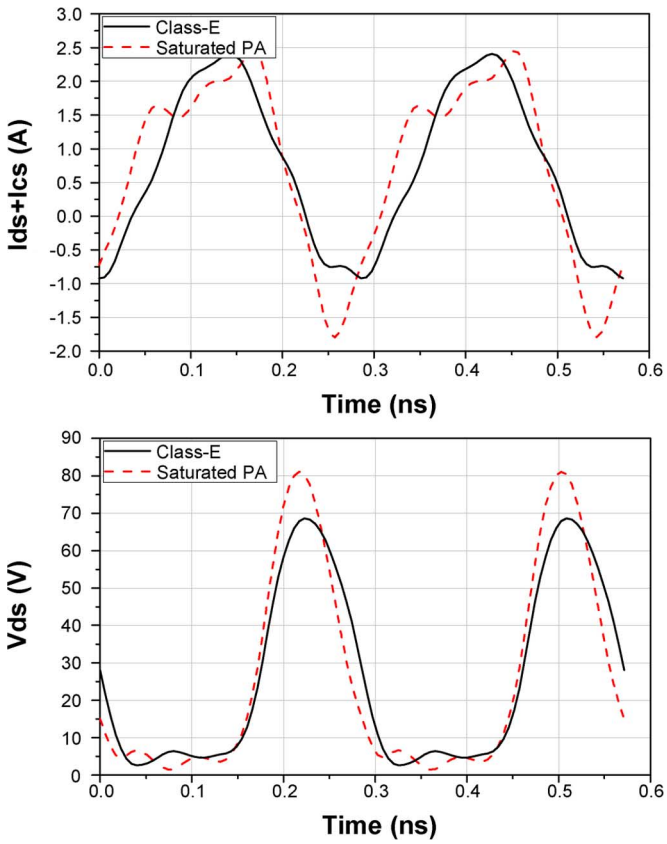

Fig. 16. Waveform of the Class-E PA and saturated amplifier for CGH40010 package device containing a Cree CGH60010 bare chip model.

C. Implementation and Experimental Results

The saturated amplifier is implemented using a Cree GaN HEMT CGH40010 package device containing a Cree CGH60015 bare chip since we cannot handle the bare chip properly. The previous simulation is carried out using the packaged device model and the waveform are depicted in Fig. 16. The waveforms are very similar to that of the CGH60015 bare chip case. Using the simulation result, the saturated amplifier was implemented at 3.5 GHz. Fig. 17 shows a photograph of the designed saturated amplifier implemented on a Taconic TLY-5 substrate with $\varepsilon_r = 2.2$ and a thickness of 31 mil. In the experiment, the gate bias is set to -2.74 V ($I_{\mathrm{DSQ}} = 50$ mA) at a supply drain voltage V_{DC} of 26 V. To validate the simulation result, the simulated and measured S-parameters are compared

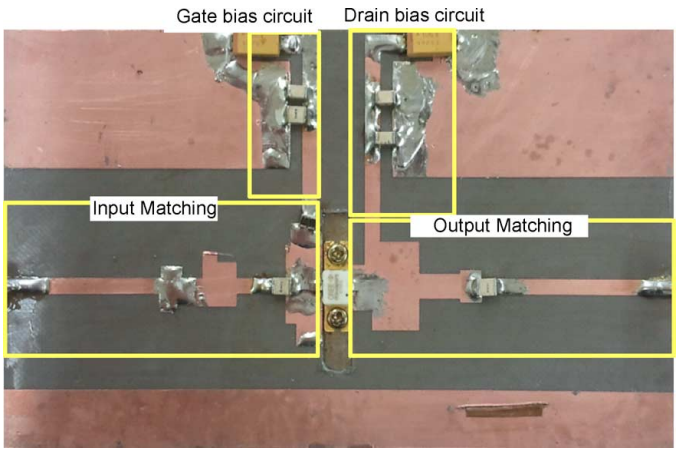

Fig. 17. Photograph of the designed saturated amplifier.

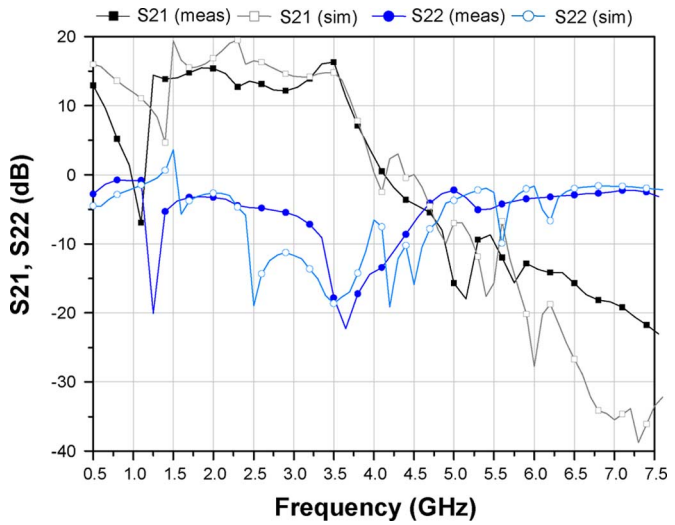

Fig. 18. Simulated and measured S-parameters of the saturated amplifier.

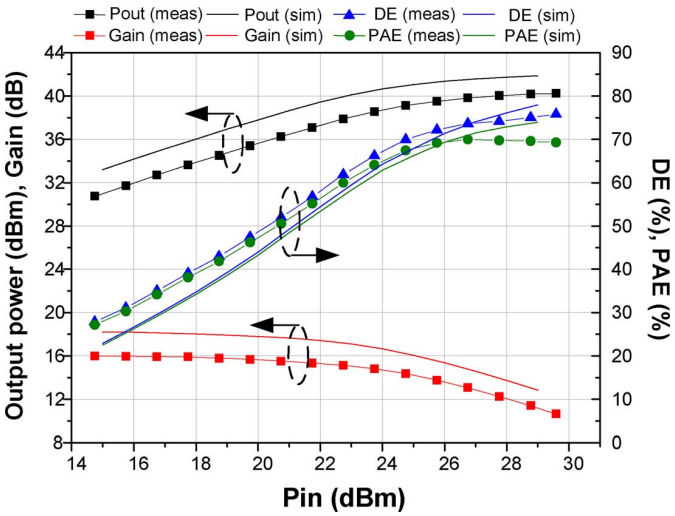

Fig. 19. Simulated and measured output performances of the saturated amplifier.

at a frequency band from 0.5 to 7.5 GHz in Fig. 18. The measured S-parameters are very similar to the simulated one. The simulated and measured output power, drain efficiency (DE), PAE, and gain are also well matched, as shown in Fig. 19. The peak drain efficiency of 75.8% is obtained at a saturated output power of 40.2 dBm.

V. Conclusion

The ideal Class-E operation that can deliver 100% efficiency is investigated. Even in the ideal operation at a low frequency, the capacitor cannot be charged sufficiently quickly, thus degrading the efficiency. The ideal Class-E operation is not possible at high frequencies because the discharging process is not sufficiently fast, further restricting the ideal switching. To obtain higher output power and efficiency for the operation above $f_{\max,E}$, the Class-E PA is optimized using load-pull simulation. The best efficiency is obtained from the bifurcated current waveform at the saturated operation. The Class-E PA with nonlinear $C_{\rm out}$ and $C_{\rm in}$ for operation above $f_{\max,E}$ is analyzed and optimized for high efficiency. It is shown that the nonlinear output capacitor enhances the efficiency due to the out-of-phase second-harmonic voltage generation. The further optimized Class-E PA becomes the saturated amplifier. The main difference in the circuit is the inductive second-harmonic load, tuning out the output capacitor at the second harmonic and the power-matched fundamental load. Although the Class-E PA operates in the switching mode even above $f_{\max,E}$, the saturated PA is a gm-driven mode. The saturated amplifier delivers the higher performance with well-shaped half-sinusoidal voltage waveform and a less bifurcated current waveform. The saturated amplifier is implemented at 3.5 GHz using a Cree GaN HEMT CGH40010 device. It provides a drain efficiency of 75.8% at a saturated power of 40.2 dBm (10.5 W).

Acknowledgment

The authors would like to thank Cree for providing the transistors and the large-signal model of GaN HEMT used in this study.

References

[1] S. C. Cripps, *RF Power Amplifiers for Wireless Communications*. Norwood, MA: Artech House, 2006.
[2] F. H. Raab, "Class-F power amplifiers with maximally flat waveforms," *IEEE Trans. Microw. Theory Tech.*, vol. 45, no. 11, pp. 2007–2012, Nov. 1997.
[3] S. Gao, "High-efficiency class-F RF/microwave power amplifiers," *IEEE Microw. Mag.*, vol. 7, no. 1, pp. 40–48, Feb. 2006.
[4] Y. Y. Woo, Y. Yang, and B. Kim, "Analysis and experiments for high-efficiency Class-F and inverse Class-F power amplifiers," *IEEE Trans. Microw. Theory Tech.*, vol. 54, no. 5, pp. 1969–1974, May 2006.
[5] S. C. Cripps, P. J. Tasker, A. L. Clarke, J. Lees, and J. Benedikt, "On the continuity of high efficiency modes in linear RF power amplifiers," *IEEE Microw. Wireless Compon. Lett.*, vol. 19, no. 10, pp. 665–667, Oct. 2009.
[6] N. O. Sokal and A. D. Sokal, "Class-E: A new class of high-efficiency tuned single-ended switching power amplifiers," *IEEE J. Solid-State Circuits*, vol. SC-10, pp. 168–176, Jun. 1975.
[7] F. H. Raab, "Idealized operation of the Class-E tuned power amplifier," *IEEE Trans. Circuit Syst.*, vol. CAS-24, no. 12, pp. 725–735, Jun. 1975.
[8] J. Moon, J. Kim, and B. Kim, "Investigation of a Class-J power amplifier with a nonlinear $C_{\rm out}$ for optimized operation," *IEEE Trans. Microw. Theory Tech.*, vol. 58, no. 11, pp. 2800–2811, Nov. 2010.
[9] P. Colantonio, F. Giannini, G. Leuzzi, and E. Limiti, "High efficiency low-voltage power amplifier design by second-harmonic manipulation," *Int. J. RF Microw. Comput.-Aided Eng.*, vol. 10, no. 1, pp. 19–32, 2000.

[10] P. Colantonio, F. Giannini, G. Leuzzi, and E. Limiti, "Class G approach for high efficiency PA design," *Int. J. RF Microw. Comput.-Aided Eng.*, vol. 10, no. 6, pp. 366–378, Nov. 2000.
[11] P. Colantonio, F. Giannini, and E. Limiti, *High Efficiency RF and Microwave Solid State Power Amplifiers*. Hoboken, NJ: Wiley, 2009.
[12] P. Saad, H. Nemati, K. Andersson, and C. Fager, "Highly efficient GaN-HEMT power amplifiers at 3.5 GHz and 5.5 GHz," in *Proc. 12th Wireless Microw. Technology Conf.*, Apr. 2011, pp. 1–4.
[13] T. B. Madar, E. W. Bryerton, M. Markovic, M. Forman, and Z. Popovic, "Switched-mode high-efficiency microwave power amplifier in a free-space power-combiner array," *IEEE Trans. Microw. Theory Tech.*, vol. 46, no. 10, pp. 1391–1398, Oct. 1998.
[14] E. Cipriani, P. Colantonio, F. Giannini, and R. Giofre, "Theory and experimental validation of a Class E PA above theoretical maximum frequency," *Int. J. Microw. Wireless Tech.*, vol. 1, no. 4, pp. 293–299, Jun. 2009.
[15] E. Cipriani, P. Colantonio, F. Giannini, and R. Giofre, "Optimization of Class E power amplifiers above theoretical maximum frequency," in *Posc. 38th IEEE Eur. Microw. Conf.*, Oct. 2008, pp. 1541–1544.
[16] R. Pengelly, B. Million, D. Farrel, B. Pribble, and S. Wood, "Application of non-linear models in a range of challenging GaN HEMT power amplifier design," in *IEEE MTT-S Int. Microw. Symp. Dig*, Jun. 2008.
[17] T. Suetsugu and M. K. Kazimierczuk, "Comparison of Class-E amplifier with nonlinear and linear shunt capacitance," *IEEE Trans. Circuit Syst. I, Fundam. Theory Appl.*, vol. 50, no. 8, pp. 1089–1097, Aug. 2003.
[18] A. Mediano, P. M. Gaudo, and C. Bernal, "Design of Class-E amplifier with nonlinear and linear shunt capacitances for any duty cycle," *IEEE Trans. Microw. Theory Tech.*, vol. 55, no. 3, pp. 484–492, Mar. 2007.
[19] B. Kim, J. Moon, and J. Kim, "Highly efficient saturated power amplifier assisted by nonlinear output capacitor," in *IEEE MTT-S Int. Microw. Symp. Dig.*, May 2010.
[20] J. Kim, J. Kim, J. Moon, J. Son, I. Kim, S. Jee, and B. Kim, "Saturated power amplifier optimized for efficiency using self-generated harmonic current and voltage," *IEEE Trans. Microw. Theory Tech.*, vol. 59, no. 8, pp. 2049–2058, Aug. 2011.

Seunghoon Jee received the B.S. degree in electronic and electrical engineering from Kyungpook National University, Daegu, Korea, in 2009. He is currently working toward the Ph.D. degree at the Pohang University of Science and Technology (POSTECH), Pohang, Korea.

His current research interests include highly linear and efficient RF power-amplifier design.

Junghwan Moon (S'07) received the B.S. degree in electrical and computer engineering from the University of Seoul, Seoul, Korea, in 2006. He is currently working toward the Ph.D. degree at the Pohang University of Science and Technology (POSTECH), Pohang, Korea.

His current research interests include highly linear and efficient RF power-amplifier (PA) design, memory-effect compensation techniques, digital predistortion (DPD) techniques, and wideband RF PA design.

Mr. Moon was the recipient of the Highest Efficiency Award at the Student High-Efficiency Power Amplifier Design Competition at the IEEE Microwave Theory and Techniques Society (IEEE MTT-S) International Microwave Symposium (IMS) in 2008 and the First Place Award at Student High-Efficiency Power Amplifier Design Competition at IEEE MTT-S IMS in 2011.

Jungjoon Kim received the B.S. degree from Han-Yang University, Ansan, Korea, in 2007, and the M.S. degree in from the Pohang University of Science and Technology (POSTECH), Pohang, Korea, in 2009, both in electrical engineering. He is currently working toward the Ph.D. degree at the POSTECH, Pohang, Korea.

His current research interests include RF power-amplifier design and supply modulator design for highly efficient transmitter systems.

Junghwan Son received the B.S. degree in physics from Sejong University, Seoul, Korea, in 2008, and the M.S. degree in computer and communications engineering in from the Pohang University of Science and Technology (POSTECH), Pohang, Korea, in 2010. He is currently working toward the Ph.D. degree in electrical and electronics engineering at POSTECH.

His current research interests include RF power-amplifier design and linearity.

Bumman Kim (M'78–SM'97–F'07) received the Ph.D. degree in electrical engineering from Carnegie Mellon University, Pittsburgh, PA, in 1979.

From 1978 to 1981, he was engaged in fiber-optic network component research with GTE Laboratories Inc. In 1981, he joined the Central Research Laboratories, Texas Instruments Inc., where he was involved in development of GaAs power field-effect transistors (FETs) and monolithic microwave integrated circuits (MMICs). He has developed a large-signal model of a power FET, dual-gate FETs for gain control, high-power distributed amplifiers, and various millimeter-wave MMICs. In 1989, he joined the Pohang University of Science and Technology (POSTECH), Pohang, Korea, where he is a POSTECH Fellow and a Namko Professor with the Department of Electrical Engineering, and Director of the Microwave Application Research Center, where he is involved in device and circuit technology for RF integrated circuits (RFICs). He has authored over 300 technical papers.

Prof. Kim is a member of the Korean Academy of Science and Technology and the National Academy of Engineering of Korea. He was an associate editor for the IEEE TRANSACTIONS ON MICROWAVE THEORY AND TECHNIQUES, a Distinguished Lecturer of the IEEE Microwave Theory and Techniques Society (IEEE MTT-S), and an AdCom member.